Multicondensate lengths with degenerate excitation gaps in $BaNi_2As_2$ revealed by muon spin relaxation study

Kaiwen Chen,[1] Zihao Zhu,[1] Yaofeng Xie,[2] Adrian D. Hillier,[3] James S. Lord,[3] Pengcheng Dai,[2] and Lei Shu[1,4,*]

[1]*Department of Physics, State Key Laboratory of Surface Physics, Fudan University, Shanghai 200438, China*

[2]*Department of Physics and Astronomy, Rice University, Houston, Texas 77005, USA*

[3]*ISIS Facility, STFC Rutherford Appleton Laboratory, Harwell Science and Innovation Campus, Didcot OX11 0QX, United Kingdom*

[4]*Shanghai Research Center for Quantum Sciences, Shanghai 201315, China*

(Received 28 September 2023; revised 5 January 2024; accepted 8 January 2024; published 29 January 2024)

The recently discovered (Ba,Sr)Ni_2As_2 family provides an ideal platform for investigating the interaction between electronic nematicity and superconductivity. Here, we report the muon spin relaxation (μSR) measurements on $BaNi_2As_2$. Transverse-field μSR experiments indicate that the temperature dependence of superfluid density is best fitted with a single-band *s*-wave model. On the other hand, the magnetic penetration depth λ shows magnetic field dependence, which contradicts the single-band fully gapped scenario. Zero-field μSR experiments indicate the absence of spontaneous magnetic field in the superconducting state, showing the preservation of time-reversal symmetry in the superconducting state. Our μSR experiments suggest that $BaNi_2As_2$ is a fully gapped multiband superconductor. The superconducting gap amplitudes of each band are nearly the same while different bands exhibit different coherence lengths. The present work helps to elucidate the controversial superconducting property of this parent compound, paving the way for further research on doping the system with Sr to enhance superconductivity.

DOI: 10.1103/PhysRevB.109.024513

I. INTRODUCTION

One of the core issues in quantum materials is how superconductivity interacts with the Fermi surface instabilities such as charge density wave (CDW) and nematic order (NO) [1–3]. Although the CDWs in cuprates have been discovered for nearly three decades [4], their contribution to anomalous superconducting properties has not yet been thoroughly understood [5–7]. In the Fe-based superconductors, the nematic order causing C_4-rotational symmetry breaking strongly intertwines with the spin density wave [8–10]. By suppressing these orders with pressure or doping, the superconductivity appears and is maximally enhanced near the nematic and/or magnetic quantum critical point (QCP) [11,12]. However, the entanglement between plural electronic instabilities complicates our understanding of the relationship between enhanced superconducting pairing and such instabilities.

Enormous efforts have been made to elucidate the physics of Fe-based superconductors. In this process, many other superconducting systems were discovered [13–15]. Among them, the nickel-based $BaNi_2As_2$, which shares the same high-temperature tetragonal structure with the intensively studied 122 iron arsenide superconductors [16–19], has attracted attention recently. Compared to its iron analog, which does not superconduct without doping at ambient pressure, $BaNi_2As_2$ itself shows superconductivity below $T_c \sim 0.6$ K [20] and undergoes a structure transition into a triclinic phase near $T^* \sim 130$ K [21]. An increasing number of recent studies have revealed an exotic normal state, characterized by complex charge density instabilities [22–24] and dynamic nematic fluctuations [25]. Though early studies on electronic properties have led to conventional BCS superconductivity [26,27], substituting Ba with Sr can boost T_c from 0.6 K to 3.6 K with the suppression of structural transition to zero temperature, which indicates the possible nematic-enhanced superconductivity near the optimal doping [28,29]. Therefore, $BaNi_2As_2$ provides an ideal platform to study how nematic fluctuation itself can influence superconductivity, as there is no magnetic order or spin fluctuations in the system.

Up to now, most of the studies on $BaNi_2As_2$ are focused on the driving force of structure transition or the origin of CDWs. In fact, the nature of superconductivity of $BaNi_2As_2$ is still unclear. On the one hand, early *ab initio* band structure calculation [27] and angle-resolved photoemission spectroscopy (ARPES) measurements [30] have revealed the presence of multiple bands crossing the Fermi level. The S-shaped field dependence of thermal conductivity suggested multiple nodeless superconducting gaps [31]. On the other hand, both specific-heat and thermal conductivity studies exclude the appearance of a second gap [20,31]. For unconventional superconductors coexisting with several electronic instabilities, the multiband property is a crucial ingredient since it is closely related to the pairing mechanism [32]. Therefore, it is important to determine the superconducting property of $BaNi_2As_2$.

Muon-spin relaxation/rotation (μSR) is a powerful technique to study the gap symmetry of superconductors by providing direct information on magnetic penetration depth λ [33,34]. In this work, transverse-field (TF) μSR experiments have been performed to study the temperature and magnetic

*leishu@fudan.edu.cn

field dependence of λ of $BaNi_2As_2$. The temperature dependence of superfluid density ρ_s is well fitted with a single-band *s*-wave function with zero temperature gap amplitude $\Delta_0 = 0.101(6)$ meV. On the other hand, the field dependence of muon spin relaxation rates is well fitted with a two-band model. Furthermore, λ shows a magnetic field dependence, contradicting the single-band fully gapped scenario. Our TF-μSR results suggest that $BaNi_2As_2$ is a multiband fully gapped superconductor with equal gap value but different coherence lengths in each band. The zero-field (ZF) μSR experiments reveal that the time-reversal symmetry is preserved in the superconducting state of $BaNi_2As_2$.

II. EXPERIMENTAL DETAILS

High-quality single crystals of $BaNi_2As_2$ were synthesized at Rice University with the same procedure described in Ref. [20]. The single-crystal x-ray diffraction (XRD) experiment suggested the high purity of our samples.

The μSR experiments were carried out on the MuSR spectrometer at the ISIS Neutron and Muon Facility, Rutherford Appleton Laboratory, Chilton, UK. Several pieces of single crystals were mounted on the high-purity silver plate with diluted GE varnish. The experiments were carried out in temperatures ranging from 50 mK to 1.0 K for both the ZF- and TF-μSR setup. TF-μSR experiments were performed under external magnetic fields from 5 mT to 40 mT. The sample was field cooled above T_c to base temperature in order to form an ideal vortex lattice. All the μSR spectra were collected upon warming and the data were analyzed with the MUSRFIT software package [35].

III. RESULTS

A. Zero-field muon spin relaxation

The ZF-μSR measurement was performed to figure out the magnetic ground state of $BaNi_2As_2$ and to examine whether the superconducting transition was accompanied by an additional break of time-reversal symmetry. Two representative ZF-μSR spectra measured above and below T_c are shown in Fig. 1. No oscillations or loss of initial asymmetry were observed, suggesting the absence of both long-range and short-range magnetic order down to 70 mK. This is consistent with the previous neutron scattering study [36]. ZF muon spin asymmetry spectra after subtracting the background signal A_{ZF} can be well fitted with a damped Gaussian Kubo-Toyabe (KT) function [37]:

$$A_{ZF}(t) = A_0(T)G_{KT}(\sigma_{ZF}, t)e^{-\lambda t}. \quad (1)$$

The KT term describes a Gaussian distribution of randomly oriented static (or quasi-static) local fields at muon sites with distribution width $\delta B_G = \sigma_{ZF}/\gamma_\mu$, where $\gamma_\mu = 2\pi \times 135.53$ MHz/T is the muon gyromagnetic ratio [38]:

$$G_{KT}(\sigma_{ZF}, t) = \frac{1}{3} + \frac{2}{3}\left(1 - \sigma_{ZF}^2 t^2\right)\exp\left(-\frac{1}{2}\sigma_{ZF}^2 t^2\right). \quad (2)$$

The exponential term represents the additional electronic depolarization rate [37]. σ_{ZF} is found to show little temperature dependence and is fixed to the average value of $\sigma_{ZF} = 0.122$ μs^{-1} during the fitting. The temperature dependence of λ is displayed in Fig. 1(b). Though λ grows at the lowest temperature, whose origin is not clear based on the present data, it does not show obvious change crossing T_c. The current ZF-μSR result suggests that no spontaneous time-reversal symmetry breaking exists with superconducting transition.

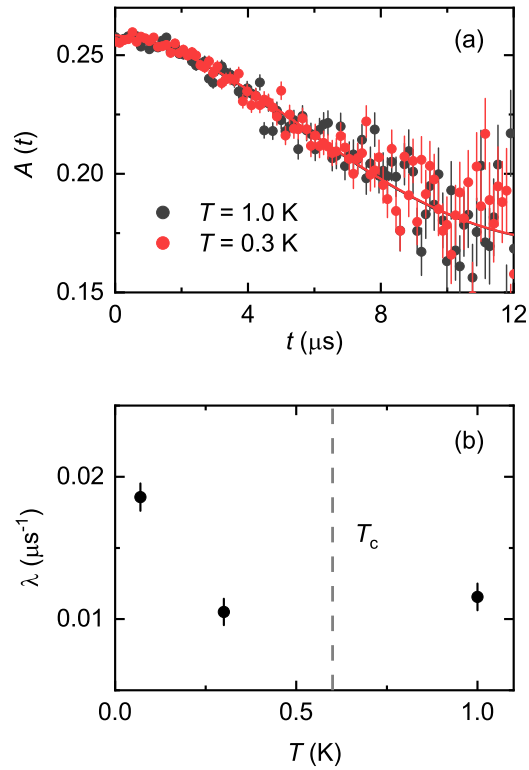

FIG. 1. (a) ZF muon decay positron asymmetry $A(t)$, proportional to the muon spin polarization, measured in the normal state (black circles) and the superconducting state (red circles), respectively. The solid curves are the fits of data with Eq. (1). (b) Temperature dependence of muon spin relaxation rate λ down to 70 mK. The gray dashed line indicates the superconducting critical temperature T_c.

B. Transverse-field muon spin relaxation

To elucidate the pairing symmetry and the band character of superconductivity in $BaNi_2As_2$, systematic temperature-dependent μSR experiments were performed under several transverse magnetic fields from 5 mT to 40 mT. The lower critical field H_{c1} of $BaNi_2As_2$ is estimated with [39]

$$H_{c1} = H_{c2}\frac{\ln\kappa + 0.497}{2\kappa^2}. \quad (3)$$

Considering $\kappa \approx 11$ estimated from normal state thermal conductivity [31], Eq. (3) gives $H_{c1} \approx 1.3$ mT. Although this is only an estimation, the applied magnetic field of 5 mT is large enough to form the uniform vortex lattice in $BaNi_2As_2$.

Two representative TF-μSR spectra above and below T_c are shown in Fig. 2. The damping of asymmetry is enhanced after entering the superconducting state, indicating the bulk superconductivity of our sample. The superconducting volume fraction can be estimated from the difference of long-time spectra [40]. However, the relaxation of asymmetry spectra is relatively slow in $BaNi_2As_2$, and its asymmetry spectra failed

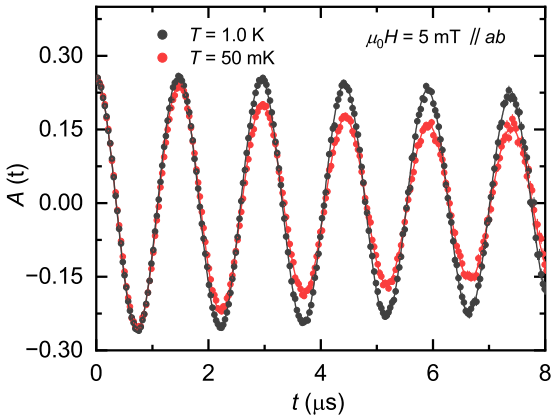

FIG. 2. TF-μSR asymmetry spectra measured at $\mu_0 H = 5$ mT. The black and red circles represent the asymmetry spectra in the normal state and in the superconducting state, respectively. The solid curves are the fits of data with Eq. (4).

to fully relax even when the data points started to diverge (after 8 μs, not shown). Nevertheless, based on the asymmetry spectra at 8 μs, the lower limit of superconducting volume fraction can be estimated to be about 75%.

The TF-μSR data is analyzed with the function

$$A(t)/A_0 = \left[(1-f)\exp(-\sigma^2 t^2/2)\cos(\gamma_\mu \mu_0 H_{\rm int} + \phi) + f\exp\left(-\sigma_{\rm bg}^2 t^2\right)\cos(\gamma_\mu \mu_0 H_{\rm bg} + \phi)\right], \quad (4)$$

where A_0 stands for the initial asymmetry; f represents the proportion of the background signal and $(1-f)$ represents the proportion of sample signal; σ is the Gaussian relaxation rate, which is related to the Gaussian field distribution in the sample; $\mu_0 H_{\rm int}$ is the average field sensed by muons stopping in the sample; $\sigma_{\rm bg}$ is the relaxation rate of muon stopping in the silver, which is temperature independent and is fixed during the fitting [41,42]; $\mu_0 H_{\rm bg}$ is the field sensed by muon stopping in the background, and ϕ is the shared initial phase.

The extracted relaxation rates σ with Eq. (4) are displayed in Fig. 3(a). For $T > T_c$, the muon relaxation rates are almost the same under different temperatures and magnetic fields, as expected for muon depolarization by the randomly oriented nuclear dipole moments in the sample. The muon spin relaxation rates are greatly enhanced after entering the superconducting state due to the inhomogenous magnetic field distribution of the flux-line lattice (FLL) [43]. The contribution from the flux-line lattice adds in quadrature to the contribution of nuclear dipole moment of the sample:

$$\sigma^2 = \sigma_{\rm dip}^2 + \sigma_{\rm FLL}^2, \quad (5)$$

where $\sigma_{\rm dip}$ is the contribution from the randomly oriented nuclear dipolar moments and $\sigma_{\rm FLL}$ is the flux-line lattice contribution. The temperature dependence of the extracted $\sigma_{\rm FLL}$ using Eq. (5) is plotted in Fig. 3(b). The behavior that σ does not change from the base temperature to $T \sim T_c/3$ suggests the fully gapped superconductivity in $BaNi_2As_2$.

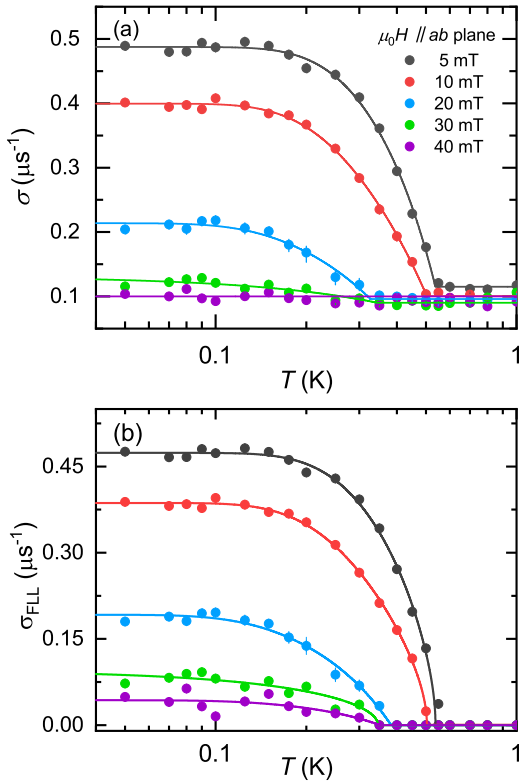

FIG. 3. Temperature dependence of muon spin relaxation rates (a) σ and (b) $\sigma_{\rm FLL}$ under different external fields, respectively. The solid lines are guides for the eyes.

C. Magnetic field and temperature dependence of magnetic penetration depth

The internal field distribution of type-II superconductors can be described by the penetration depth λ and coherence length ξ [39]. For a type-II superconductor with $\kappa \geqslant 5$ and a moderate reduced magnetic field $h = H/H_{c2} > 0.25/\kappa^{1.3}$, λ can be calculated with the numerical Ginzburg-Landau model with less than 5% error [39]:

$$\sigma_{\rm FLL}[\mu s^{-1}] = 4.83 \times 10^4 (1-h) \times [1 + 1.21(1-\sqrt{h})^3]\lambda^{-2}[nm^{-2}]. \quad (6)$$

Noting that the muon spin relaxation rate is nearly temperature independent below $T = 0.1$ K, it is reasonable to analyze the field dependence of $\sigma_{\rm FLL}$ at base temperature with the zero-temperature upper critical field $H_{c2}^{ab}(0) = 0.11$ T taken from Ref. [31]. The superscript here indicates that the direction of the external field is in the *ab* plane. For conventional single-band *s*-wave superconductors with medium κ, the value of $\lambda^{-2}(T)$ and $H_{c2}^{ab}(T)$ can be obtained by fitting the isothermal magnetic field dependence of $\sigma_{\rm FLL}$ at different temperatures [44]. The field dependence of $\sigma_{\rm FLL}$ using Eq. (6) with fixed $H_{c2}^{ab}(0)$ at base temperature ($T = 50$ mK) is shown in the black dashed line in Fig. 4. It can be seen that the experimentally measured $\sigma_{\rm FLL}$ is far from the theoretical calculation, dropping much faster than expected for single-band *s*-wave superconductivity. Noting that the field dependence of $\sigma_{\rm FLL}$ described by Eq. (6) is only valid under the assumption of a field-independent λ [39], the deviation

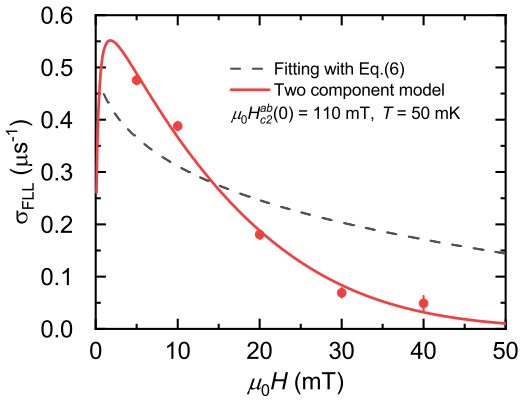

FIG. 4. The magnetic-field dependence of muon spin relaxation rate σ_{FLL}. The black dashed line is the theoretically expected σ_{FLL} with Eq. (6). The red solid line exhibits the fits of data with the two-component Ginzburg-Landau model [48], using $\xi_1^{ab} = 55.1$ nm, $\xi_2^{ab} = 71.6$ nm deduced from Refs. [20] and [31], resulting in $\lambda = 0.38(1)$ μm and $w = 0.7(1)$.

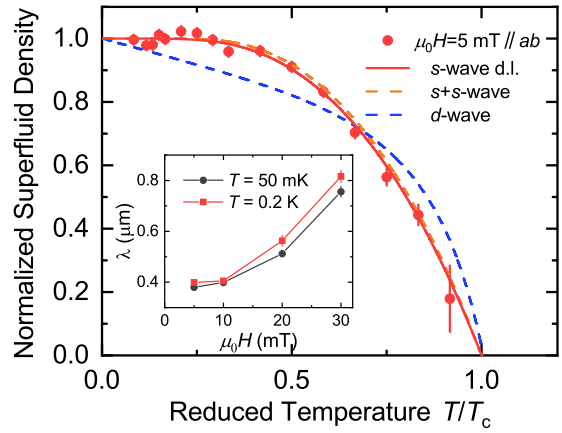

FIG. 5. Temperature dependence of the reduced superfluid density versus the reduced temperature T/T_c measured at $\mu_0 H = 5$ mT parallel to the ab plane. The colored curves stand for the fitting of Eq. (10) with different gap symmetry functions. The inset shows the field dependence of magnetic penetration depth λ at $T = 50$ mK and 0.2 K. The connecting lines in the inset are guides for the eyes.

of σ_{FLL} from the theoretical expectation indicates that λ exhibits magnetic field dependence, which is expected for superconductors with nodes or/and multiband superconductors [45–47]. Considering the multiband nature of $BaNi_2As_2$ [27,30], the field dependence of σ_{FLL} is further analyzed with the two-component modified London model [48]:

$$\overline{\Delta B^2} = \overline{B}^2 \sum_{\boldsymbol{q}\neq 0} \left[w \frac{e^{-\boldsymbol{q}^2\xi_1^2/2(1-h_1)}}{1+\boldsymbol{q}^2\lambda^2/(1-h_1)} + (1-w)\frac{e^{-\boldsymbol{q}^2\xi_2^2/2(1-h_2)}}{1+\boldsymbol{q}^2\lambda^2/(1-h_2)} \right], \tag{7}$$

where $\boldsymbol{q} = \frac{4\pi}{\sqrt{a}}(\frac{\sqrt{3}m}{2}, n+\frac{m}{2})$ are the reciprocal lattice vectors for triangular FLL ($a = 1.075\sqrt{\frac{\Phi_0}{B}}$ is the intervortex distance), ξ_i is the coherence length for the ith band, and w stands for the contribution of the first band to the total superfluid density. The cutoff function $e^{-\boldsymbol{q}^2\xi^2/2}$ is a standard approximation for Ginzburg-Landau equations introduced to account for the finite size of vortex cores [49]. Since the four parameters are strongly coupled, it is generally hard to obtain a unique set of solutions. This can be resolved by fixing ξ_i based on the reported properties. The shorter coherence length $\xi_1^{ab} \approx 55.1$ nm can be estimated by the upper critical field with $\xi_1^{ab} = [\Phi/2\pi H_{c2}^{ab}(0)]^{1/2}$. Here, $H_{c2}^{ab}(0)$ is the zero-temperature upper critical field for $H \parallel ab$. The ratio of two coherence lengths $\xi_1^{ab}/\xi_2^{ab} = \sqrt{1/0.6} \approx 1.3$ can be obtained from the thermal conductivity measurement [31], which will be discussed later. The fitting result with fixed $\xi_{1,2}^{ab}$ is shown by the solid red line in Fig. 4, giving $\lambda = 0.38(1)$ μm and $w = 0.7(1)$.

Next, we discuss the temperature dependence of λ^{-2}. For single-band s-wave superconductors with uncertain upper critical fields, $\lambda^{-2}(T)$ and $H_{c2}^{ab}(T)$ can be obtained by fitting the magnetic field dependence of muon relaxation rates under different temperatures [44], while such a method cannot be used when λ exhibits magnetic field dependence [39]. We first tried to extract $\lambda(T)$ with Eq. (7). However, the limited data points and the complexity of the formula made it hard to get reasonable results in the whole temperature range, especially when the temperatures approached T_c. To subtract the $\lambda^{-2}(T)$, Eq. (6) was used under constant magnetic field H with fixed upper critical field $H_{c2}^{ab}(T)$ [50]. With the known reduced magnetic field h, $\lambda^{-2}(T)$ can be directly calculated from σ_{FLL}.

Considering the two-band feature of $BaNi_2As_2$, the temperature dependence of H_{c2}^{ab} was estimated with the empirical two-band model [51,52],

$$H_{c2}^{ab}(T) = H_{c2}^{ab}(0)\frac{1-t^2}{1+t^2}, \tag{8}$$

where $t = T/T_c$ and $H_{c2}^{ab}(0) = 0.11$ T was measured by heat capacity [31]. Since the upper critical fields $H_{c2}^{ab}(T)$ here are estimates, we only calculate $\lambda^{-2}(T)$ at the lowest magnetic field.

D. Temperature dependence of superfluid density and gap symmetry

The superfluid density ρ_s is proportional to λ^{-2} based on the London approximation. The resulting normalized superfluid density is plotted in Fig. 5. To further study the gap symmetry of $BaNi_2As_2$, the temperature dependence of ρ_s is fitted with different gap symmetry functions in both dirty limit (d.l.),

$$\frac{\rho_s(T)}{\rho_s(0)} = \frac{\Delta(T,\phi)}{\Delta(0,\phi)}\tanh\left[\frac{\Delta(T,\phi)}{2k_BT}\right], \tag{9}$$

and clean limit (c.l.),

$$\frac{\rho_s(T)}{\rho_s(0)} = 1 + \frac{1}{\pi}\int_0^{2\pi} d\phi \int_{\Delta(T,\phi)}^{\infty} \frac{\partial f}{\partial E}\frac{E}{\sqrt{E^2-\Delta(T,\phi)^2}}dE, \tag{10}$$

where $f = [1+\exp(E/k_BT)]^{-1}$ is the Fermi function. $\Delta(T,\phi) = \Delta(\phi)\delta(T/T_c)$ is the gap symmetry function. For the s-wave model, $\Delta_s(\phi) = \Delta_0$; for the d-wave model,

TABLE I. Fitted parameters to the σ_{sc} of $BaNi_2As_2$ with different models described in the text.

Model	Gap value (meV)	T_c (K)	$2\Delta/k_BT_c$	χ_r^2
s wave c.l.	$\Delta = 0.112(3)$	0.611(8)	4.2(1)	0.98
s wave d.l.	$\Delta = 0.101(6)$	0.610(8)	3.8(2)	1.03
	$\Delta_1 = 0.110(4)$, $\Delta_2 = 0.11(1)$			
$s+s$ wave	$w = 0.95(51)$	0.603(6)	4.2(4)	1.21
d wave	$\Delta = 0.217(9)$	0.574(3)	8.8(3)	6.15

$\Delta_d = \Delta_0 \cos(2\phi)$. The temperature dependence $\delta(T/T_c)$ can be approximated as [53]

$$\delta(T/T_c) = \tanh\{1.82[1.018(T_c/T - 1)]^{0.51}\}, \quad (11)$$

where Δ_0 is the maximum zero-temperature gap amplitude.

To examine the possible multigap nature inferred from Fermi surface structure calculation [27,30] and thermal conductivity measurement [31], we also consider two weakly coupled superconducting bands ($s+s$ or $s+d$), where the linear combination of Eq. (11) can be used:

$$\frac{\lambda^{-2}(T)}{\lambda^{-2}(0)} = w\frac{\lambda^{-2}(T,\Delta_1(T))}{\lambda^{-2}(0,\Delta_1(0))} + (1-w)\frac{\lambda^{-2}(T,\Delta_2(T))}{\lambda^{-2}(0,\Delta_2(0))}. \quad (12)$$

The fitting results with different models are summarized in Fig. 5 and Table I. The temperature dependence of the normalized superfluid density can be well fitted with both the single-gap and multigap s-wave model. However, the introduction of a second gap does not seem to improve the fitting quality to a great extent, and we can hardly get a second gap value with difference exceeds the standard error. Therefore, there is no need to introduce more than one gap amplitude to describe $\lambda^{-2}(T)$. The estimated electronic mean free path in the normal state places $BaNi_2As_2$ in the dirty limit [31]. The obtained zero-temperature superconducting gap $\Delta_0 = 0.101(6)$ meV and the critical temperature $T_c = 0.610(8)$ K give $2\Delta/k_BT_c = 3.8(2)$, which is close to the BCS value of 3.54. The value of the superconducting gap is close to the value of $\Delta_0 = 0.0946$ meV obtained from the heat capacity measurement by Kurita *et al*. [31].

IV. DISCUSSION

By analyzing the temperature dependence of penetration depth alone, one may conclude that $BaNi_2As_2$ is a common s-wave superconductor, which is consistent with previous heat capacity measurement. However, in single-band s-wave superconductors, λ should be independent of magnetic field [46,54,55]. As shown in the inset of Fig. 5, λ is nearly doubled when the field is increased from 5 mT to 40 mT. Such a large change of λ cannot be attributed to the error of $H_{c2}(T)$. A field dependence of λ is expected for superconductors with nodes or/and multiband superconductors [45–47]. The former case can be excluded since the penetration depth below $T_c/3$ is temperature independent, which indicates fully gapped superconductivity. For the latter case, the carriers in one of the bands is suppressed faster than other bands, causing the change of penetration depth. Since $\sigma_{FLL}(H)$ can be well described by the two-component modified London model, combined with the single-gap nature revealed by $\rho_s(T)$, we suggest that $BaNi_2As_2$ is a multiband single-gap superconductor. The superconducting gap amplitude of each band is nearly the same while different bands exhibit diverse coherence lengths [50].

A key step in our $\lambda(H)$ analysis is to determine the ratio of different coherence lengths, which is obtained from the thermal conductivity measurement. The shoulder-like anomaly of the $\kappa_0(H)/T$ curve was initially attributed to the spread in H_{c2} [31], since there was no evidence pointing to a second superconducting band at that time. However, such S-shaped $\kappa_0(H)/T$ curves were later also found in several Ni_2X_2-based superconductors [56,57], which share the same $ThCr_2Si_2$ structure and similar electronic structure [58]. Furthermore, the ratio of different coherence lengths in different bands $\xi_1^{ab}/\xi_2^{ab} \approx 1.3$ has been confirmed by the calculated band structure [26,27] and the ARPES experiment [30]. According to the BCS theory, the coherence length is proportional to $\langle v_F\rangle/\Delta_0$. Here, $\langle v_F\rangle$ is the averaged value of the Fermi velocity, which can be estimated from the slope of bands crossing the Fermi level. There are three bands crossing the Fermi level in $BaNi_2As_2$. The ratio of their slopes is about 1 along Z-A and ~1–3 along Γ-M [26,27,30]. In consideration of the same Δ_0 of the three bands, $\xi_1^{ab}/\xi_2^{ab} = 1.3$ obtained from thermal conductivity data is reasonable.

Considering the uniform gap value in each band revealed by both μSR and thermodynamic properties [31], the multiband superconductivity in $BaNi_2As_2$ is quite unique compared with other multigap superconductors [53,59,60]. It is worth noting that, for a long time, it has been widely believed that the number of excitation gaps determines the number of contributing bands needed in a theoretical model. However, there is no necessary connection between the number of excitation gaps and the number of length scales [61]. Superconductors with multibands can be (i) single gap and single length scale [62]; (ii) multigap with single length scale [63,64]; or (iii) single gap with multi length scales, such as $SrPt_3P$ [50] and $BaNi_2As_2$ in the present study.

In most cases, strong electronic scattering in conventional dirty superconductors weakens the difference between bands. As a result, each band tends to exhibit identical superconducting behavior. A natural question here is what causes the unconventional multiband behavior in $BaNi_2As_2$. Recent density functional theory (DFT) results showed that the rebonding of As anions can induce complex structural instabilities. These low-temperature structures are similar in energy but are very different in Fermiology [65]. The competition between these bonding arrangements can possibly explain this unconventional superconducting behavior. However, such a scenario is hard to reconcile with the single-gap amplitude revealed by heat capacity [31] and μSR experiments. On the other hand, recent Raman scattering measurements revealed strong dynamic nematic fluctuations in $BaNi_2As_2$, which strongly supported the nematic enhanced superconductivity upon doping in this material [25]. Whether the unconventional single-gap multiband superconducting in $BaNi_2As_2$ is a manifestation of the interaction between superconducting and nematicity demands further confirmation.

Subsequent researches on superconducting band properties in doped systems will be very helpful to elucidate how the CDW and charge-induced nematicity interact with superconductivity.

V. CONCLUSIONS

To summarize, systematic μSR experiments have been performed to study the temperature and magnetic field dependence of penetration depth λ in $BaNi_2As_2$. The temperature-independent behavior of superfluid density ρ_s at low temperature suggests its fully gapped nature. The fitting with the single-gap *s*-wave model in the dirty limit gives the zero-temperature gap amplitude $\Delta_0 = 0.101(6)$ meV. The deviation of $\sigma_{\mathrm{FLL}}(H)$ from the single-band scenario can be understood with a two-component model with different coherence lengths in each band. Our TF-μSR results reveal that $BaNi_2As_2$ is a rare single-gap multiband superconductor. The ZF-μSR experiments confirmed the preservation of time-reversal symmetry in $BaNi_2As_2$. This work provides experimental evidence to help understand the interplay between CDW, nematicity, and superconductivity.

ACKNOWLEDGMENTS

We are grateful to the ISIS Cryogenics Group for their valuable help during the μSR experiments (Grant No. ISIS.RIB 2010283). This research was funded by the National Natural Science Foundation of China (Grant No. 12174065), the National Key Research and Development Program of China (Grant No. 2022YFA1402203), and the Shanghai Municipal Science and Technology Major Project, (Grant No. 2019SHZDZX01). The materials synthesis efforts at Rice are supported by the U.S. Department of Energy (DOE), Basic Energy Sciences (BES), under Contract No. DE-SC0012311, and the Robert A. Welch Foundation, Grant No. C-1839 (P.D.).

APPENDIX: CHARACTERIZATION MEASUREMENTS ON SAMPLES POSSIBLY EXPOSED TO THE AIR

$BaNi_2As_2$ samples are air sensitive [20]. After the μSR experiments, single crystals of $BaNi_2As_2$ were stored in a glass bottle filled with nitrogen, and were shipped from the μSR facility to our university. Due to the epidemic prevention policy, our sample got stuck in customs for several months. The single-crystal XRD and electrical resistance experiments were performed on samples which were possibly exposed to the air for some time.

The single-crystal XRD diffraction patterns were obtained using a Bruker D8 advanced x-ray diffraction spectrometer ($\lambda = 1.5418$ Å) at room temperature. Single-crystal $BaNi_2As_2$ are naturally oriented with the *c* axis normal to the plate, and the XRD patterns are shown in Fig. 6. The diffraction peaks of specific lattice planes are obvious. The lattice parameter *c* is determined via the liner fitting between the diffraction pattern index *n* and $\sin(\theta)$, which gives $c = 11.66(4)$ Å. For comparison, $c = 11.54(2)$ Å in Ref. [20].

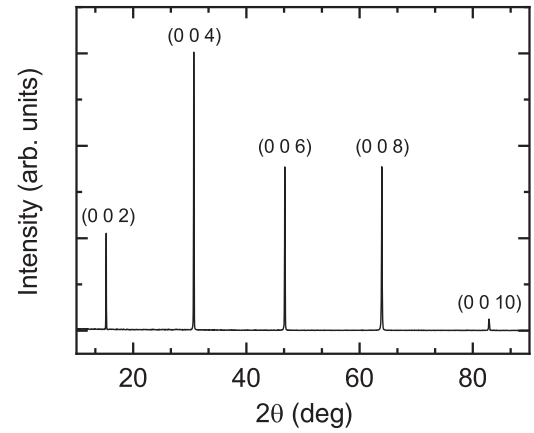

FIG. 6. Single-crystal x-ray diffraction patterns of $BaNi_2As_2$.

Temperature dependence of resistance $R(T)$ from 300 K to 0.3 K was measured using the standard four-probe method on a physical property measurement system (PPMS) equipped with a Helium3 refrigerator. The resistance was measured with cooling. Figure 7(a) shows the temperature dependence of resistance $R(T)$ from 300 K to 2 K. A broad hump is observed near 150 K, which is identified as the structural

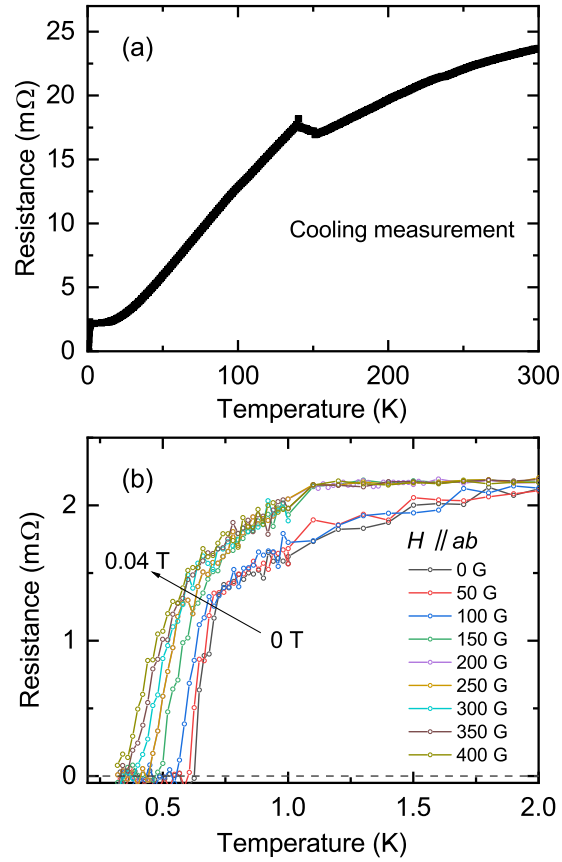

FIG. 7. Temperature dependence of resistance from 300 K to 2 K (a) and from 2.0 K to 0.3 K (b) with external magnetic field parallel to the *ab* plane. There is an additional 10 min exposure to air between the 100 G and 150 G measurements in (b).

phase transition [20]. The width of transition is much broader compared to Ref. [20], which may be due to the damage of our sample after its exposure to the air. The RRR $[= \rho(300\,\mathrm{K})/\rho(4\,\mathrm{K})]$ is 10. For comparison, RRR = 5 in Ref. [20]. The resistance below 2 K is shown in Fig. 7(b). The direction of the external magnetic field is parallel to the *ab* plane. The resistance of the sample reaches zero at 0.63 K under zero field and the sample shows superconductivity under the external field of 400 G. It should be noted that the measurements with a field higher than 100 G were conducted after the sample was exposed to the air for another 10 min. There are obvious differences between the $R-T$ curves over and below 100 G, which further illustrate that $BaNi_2As_2$ is very air sensitive.

[1] E. Fradkin, S. A. Kivelson, and J. M. Tranquada, Colloquium: Theory of intertwined orders in high temperature superconductors, Rev. Mod. Phys. **87**, 457 (2015).

[2] B. Keimer, S. A. Kivelson, M. R. Norman, S. Uchida, and J. Zaanen, From quantum matter to high-temperature superconductivity in copper oxides, Nature (London) **518**, 179 (2015).

[3] D. C. Johnston, The puzzle of high temperature superconductivity in layered iron pnictides and chalcogenides, Adv. Phys. **59**, 803 (2010).

[4] J. M. Tranquada, B. J. Sternlieb, J. D. Axe, Y. Nakamura, and S. Uchida, Evidence for stripe correlations of spins and holes in copper oxide superconductors, Nature (London) **375**, 561 (1995).

[5] H. Miao, G. Fabbris, R. J. Koch, D. G. Mazzone, C. S. Nelson, R. Acevedo-Esteves, G. D. Gu, Y. Li, T. Yilimaz, K. Kaznatcheev, E. Vescovo, M. Oda, T. Kurosawa, N. Momono, T. Assefa, I. K. Robinson, E. S. Bozin, J. M. Tranquada, P. D. Johnson, and M. P. M. Dean, Charge density waves in cuprate superconductors beyond the critical doping, npj Quantum Mater. **6**, 31 (2021).

[6] C. Proust and L. Taillefer, The remarkable underlying ground states of cuprate superconductors, Annu. Rev. Condens. Matter Phys. **10**, 409 (2019).

[7] D. F. Agterberg, J. S. Davis, S. D. Edkins, E. Fradkin, D. J. Van Harlingen, S. A. Kivelson, P. A. Lee, L. Radzihovsky, J. M. Tranquada, and Y. Wang, The physics of pair-density waves: Cuprate superconductors and beyond, Annu. Rev. Condens. Matter Phys. **11**, 231 (2020).

[8] P. Dai, Antiferromagnetic order and spin dynamics in iron-based superconductors, Rev. Mod. Phys. **87**, 855 (2015).

[9] R. M. Fernandes, A. V. Chubukov, and J. Schmalian, What drives nematic order in iron-based superconductors? Nat. Phys. **10**, 97 (2014).

[10] J. Paglione and R. L. Greene, High-temperature superconductivity in iron-based materials, Nat. Phys. **6**, 645 (2010).

[11] D. v. d. Marel, H. J. A. Molegraaf, J. Zaanen, Z. Nussinov, F. Carbone, A. Damascelli, H. Eisaki, M. Greven, P. H. Kes, and M. Li, Quantum critical behaviour in a high-T_c superconductor, Nature (London) **425**, 271 (2003).

[12] S. Lederer, Y. Schattner, E. Berg, and S. A. Kivelson, Enhancement of superconductivity near a nematic quantum critical point, Phys. Rev. Lett. **114**, 097001 (2015).

[13] M.-X. Wang, C. Liu, J.-P. Xu, F. Yang, L. Miao, M.-Y. Yao, C. Gao, C. Shen, X. Ma, X. Chen *et al.*, The coexistence of superconductivity and topological order in the Bi_2Se_3 thin films, Science **336**, 52 (2012).

[14] H. Jiang, G. Cao, and C. Cao, Electronic structure of quasi-one-dimensional superconductor $K_2Cr_3As_3$ from first-principles calculations, Sci. Rep. **5**, 16054 (2015).

[15] Q. Gu and H.-H. Wen, Superconductivity in nickel-based 112 systems, The Innovation **3**, 100202 (2022).

[16] M. Pfisterer and G. Nagorsen, Zur struktur ternärer Übergangsmetallarsenide/on the structure of ternary arsenides, Z. Naturforsch. B **35**, 703 (1980).

[17] P. L. Alireza, Y. T. C. Ko, J. Gillett, C. M. Petrone, J. M. Cole, G. G. Lonzarich, and S. E. Sebastian, Superconductivity up to 29 K in $SrFe_2As_2$ and $BaFe_2As_2$ at high pressures, J. Phys.: Condens. Matter **21**, 012208 (2009).

[18] A. Mani, N. Ghosh, S. Paulraj, A. Bharathi, and C. S. Sundar, Pressure-induced superconductivity in $BaFe_2As_2$ single crystal, Europhys. Lett. **87**, 17004 (2009).

[19] Y. Gallais, R. M. Fernandes, I. Paul, L. Chauvière, Y.-X. Yang, M.-A. Méasson, M. Cazayous, A. Sacuto, D. Colson, and A. Forget, Observation of incipient charge nematicity in $Ba(Fe_{1-x}Co_x)_2As_2$, Phys. Rev. Lett. **111**, 267001 (2013).

[20] F. Ronning, N. Kurita, E. D. Bauer, B. L. Scott, T. Park, T. Klimczuk, R. Movshovich, and J. D. Thompson, The first order phase transition and superconductivity in $BaNi_2As_2$ single crystals, J. Phys.: Condens. Matter **20**, 342203 (2008).

[21] A. S. Sefat, M. A. McGuire, R. Jin, B. C. Sales, D. Mandrus, F. Ronning, E. D. Bauer, and Y. Mozharivskyj, Structure and anisotropic properties of $BaFe_{2-x}Ni_xAs_2$ ($x = 0$, 1, and 2) single crystals, Phys. Rev. B **79**, 094508 (2009).

[22] S. Lee, G. de la Peña, S. X.-L. Sun, M. Mitrano, Y. Fang, H. Jang, J.-S. Lee, C. Eckberg, D. Campbell, J. Collini, J. Paglione, F. M. F. de Groot, and P. Abbamonte, Unconventional charge density wave order in the pnictide superconductor $Ba(Ni_{1-x}Co_x)_2As_2$, Phys. Rev. Lett. **122**, 147601 (2019).

[23] S. Lee, J. Collini, S. X.-L. Sun, M. Mitrano, X. Guo, C. Eckberg, J. Paglione, E. Fradkin, and P. Abbamonte, Multiple charge density waves and superconductivity nucleation at antiphase domain walls in the nematic pnictide $Ba_{1-x}Sr_xNi_2As_2$, Phys. Rev. Lett. **127**, 027602 (2021).

[24] Y. Guo, M. Klemm, J. S. Oh, Y. Xie, B.-H. Lei, S. Gorovikov, T. Pedersen, M. Michiardi, S. Zhdanovich, A. Damascelli, J. Denlinger, M. Hashimoto, D. Lu, S.-K. Mo, R. G. Moore, R. J. Birgeneau, D. J. Singh, P. Dai, and M. Yi, Spectral evidence for unidirectional charge density wave in detwinned $BaNi_2As_2$, Phys. Rev. B **108**, L081104 (2023).

[25] Y. Yao, R. Willa, T. Lacmann, S.-M. Souliou, M. Frachet, K. Willa, M. Merz, F. Weber, C. Meingast, R. Heid, A.-A. Haghighirad, J. Schmalian, and M. Le Tacon, An electronic nematic liquid in $BaNi_2As_2$, Nat. Commun. **13**, 4535 (2022).

[26] I. R. Shein and A. L. Ivanovskii, Electronic and structural properties of low-temperature superconductors and ternary pnictides ANi_2Pn_2 (A = Sr, Ba and Pn = P, As), Phys. Rev. B **79**, 054510 (2009).

[27] A. Subedi and D. J. Singh, Density functional study of $BaNi_2As_2$: Electronic structure, phonons, and electron-phonon superconductivity, Phys. Rev. B **78**, 132511 (2008).

[28] C. Eckberg, D. J. Campbell, T. Metz, J. Collini, H. Hodovanets, T. Drye, P. Zavalij, M. H. Christensen, R. M. Fernandes, S. Lee *et al.*, Sixfold enhancement of superconductivity in a tunable electronic nematic system, Nat. Phys. **16**, 346 (2020).

[29] S. Lederer, E. Berg, and E.-A. Kim, Tests of nematic-mediated superconductivity applied to $Ba_{1-x}Sr_xNi_2As_2$, Phys. Rev. Res. **2**, 023122 (2020).

[30] B. Zhou, M. Xu, Y. Zhang, G. Xu, C. He, L. X. Yang, F. Chen, B. P. Xie, X.-Y. Cui, M. Arita, K. Shimada, H. Namatame, M. Taniguchi, X. Dai, and D. L. Feng, Electronic structure of $BaNi_2As_2$, Phys. Rev. B **83**, 035110 (2011).

[31] N. Kurita, F. Ronning, Y. Tokiwa, E. D. Bauer, A. Subedi, D. J. Singh, J. D. Thompson, and R. Movshovich, Low-temperature magnetothermal transport investigation of a Ni-based superconductor $BaNi_2As_2$: Evidence for fully gapped superconductivity, Phys. Rev. Lett. **102**, 147004 (2009).

[32] S. Kittaka, Y. Aoki, Y. Shimura, T. Sakakibara, S. Seiro, C. Geibel, F. Steglich, H. Ikeda, and K. Machida, Multiband superconductivity with unexpected deficiency of nodal quasiparticles in $CeCu_2Si_2$, Phys. Rev. Lett. **112**, 067002 (2014).

[33] A. D. Hillier, S. J. Blundell, I. McKenzie, I. Umegaki, L. Shu, J. A. Wright, T. Prokscha, F. Bert, K. Shimomura, A. Berlie *et al.*, Muon spin spectroscopy, Nat. Rev. Methods Primers **2**, 5 (2022).

[34] J. E. Sonier, J. H. Brewer, and R. F. Kiefl, μSR studies of the vortex state in type-II superconductors, Rev. Mod. Phys. **72**, 769 (2000).

[35] A. Suter and B. Wojek, Musrfit: A free platform-independent framework for μSR data analysis, Phys. Procedia **30**, 69 (2012).

[36] K. Kothapalli, F. Ronning, E. D. Bauer, A. J. Schultz, and H. Nakotte, Single-crystal neutron diffraction studies on Ni-based metal-pnictide superconductor $BaNi_2As_2$, J. Phys.: Conf. Ser. **251**, 012010 (2010).

[37] A. Yaouanc and P. Dalmas de Réotier, *Muon Spin Rotation, Relaxation, and Resonance: Applications to Condensed Matter* (Oxford University Press, Oxford, UK, 2011).

[38] R. S. Hayano, Y. J. Uemura, J. Imazato, N. Nishida, T. Yamazaki, and R. Kubo, Zero-and low-field spin relaxation studied by positive muons, Phys. Rev. B **20**, 850 (1979).

[39] E. H. Brandt, Properties of the ideal Ginzburg-Landau vortex lattice, Phys. Rev. B **68**, 054506 (2003).

[40] F. H. Combley, Muon spin rotation spectroscopy: Principles and applications in solid state physics, Phys. Bull. **36**, 430 (1985).

[41] J. F. Bueno, D. J. Arseneau, R. Bayes, J. H. Brewer, W. Faszer, M. D. Hasinoff, G. M. Marshall, E. L. Mathie, R. E. Mischke, G. D. Morris, K. Olchanski, V. Selivanov, and R. Tacik, Longitudinal muon spin relaxation in high-purity aluminum and silver, Phys. Rev. B **83**, 205121 (2011).

[42] J. Zhang, Z. Ding, C. Tan, K. Huang, O. O. Bernal, P.-C. Ho, G. D. Morris, A. D. Hillier, P. K. Biswas, S. P. Cottrell, H. Xiang, X. Yao, D. E. MacLaughlin, and L. Shu, Discovery of slow magnetic fluctuations and critical slowing down in the pseudogap phase of $YBa_2Cu_3O_y$, Sci. Adv. **4**, eaao5235 (2018).

[43] G. Aeppli, R. J. Cava, E. J. Ansaldo, J. H. Brewer, S. R. Kreitzman, G. M. Luke, D. R. Noakes, and R. F. Kiefl, Magnetic penetration depth and flux-pinning effects in high-T_c superconductor $La_{1.85}Sr_{0.15}CuO$, Phys. Rev. B **35**, 7129 (1987).

[44] J. A. T. Barker, D. Singh, A. Thamizhavel, A. D. Hillier, M. R. Lees, G. Balakrishnan, D. M. Paul, and R. P. Singh, Unconventional superconductivity in La_7Ir_3 revealed by muon spin relaxation: Introducing a new family of noncentrosymmetric superconductor that breaks time-reversal symmetry, Phys. Rev. Lett. **115**, 267001 (2015).

[45] J. E. Sonier, R. F. Kiefl, J. H. Brewer, J. Chakhalian, S. R. Dunsiger, W. A. MacFarlane, R. I. Miller, A. Wong, G. M. Luke, and J. W. Brill, Muon-spin rotation measurements of the magnetic field dependence of the vortex-core radius and magnetic penetration depth in $NbSe_2$, Phys. Rev. Lett. **79**, 1742 (1997).

[46] R. Kadono, Field-induced quasiparticle excitations in novel type II superconductors, J. Phys.: Condens. Matter **16**, S4421 (2004).

[47] S. Weyeneth, M. Bendele, R. Puzniak, F. Murányi, A. Bussmann-Holder, N. D. Zhigadlo, S. Katrych, Z. Bukowski, J. Karpinski, A. Shengelaya, R. Khasanov, and H. Keller, Field-dependent superfluid density in the optimally doped $SmFeAsO_{1-x}F_y$ superconductor, Europhys. Lett. **91**, 47005 (2010).

[48] S. Serventi, G. Allodi, R. De Renzi, G. Guidi, L. Romanò, P. Manfrinetti, A. Palenzona, Ch. Niedermayer, A. Amato, and Ch. Baines, Effect of two gaps on the flux-lattice internal field distribution: Evidence of two length scales in $Mg_{1-x}Al_xB_2$ from μSR, Phys. Rev. Lett. **93**, 217003 (2004).

[49] J. E. Sonier, Muon spin rotation studies of electronic excitations and magnetism in the vortex cores of superconductors, Rep. Prog. Phys. **70**, 1717 (2007).

[50] R. Khasanov, A. Amato, P. K. Biswas, H. Luetkens, N. D. Zhigadlo, and B. Batlogg, $SrPt_3P$: A two-band single-gap superconductor, Phys. Rev. B **90**, 140507(R) (2014).

[51] X. Zhu, H. Yang, L. Fang, G. Mu, and H.-H. Wen, Upper critical field, Hall effect and magnetoresistance in the iron-based layered superconductor $LaFeAsO_{0.9}F_{0.1-\delta}$, Supercond. Sci. Technol. **21**, 105001 (2008).

[52] A. Changjan and P. Udomsamuthirun, The critical magnetic field of anisotropic two-band magnetic superconductors, Solid State Commun. **151**, 988 (2011).

[53] A. Carrington and F. Manzano, Magnetic penetration depth of MgB_2, Phys. C (Amsterdam, Neth.) **385**, 205 (2003).

[54] R. Khasanov, D. G. Eshchenko, D. Di Castro, A. Shengelaya, F. La Mattina, A. Maisuradze, C. Baines, H. Luetkens, J. Karpinski, S. M. Kazakov, and H. Keller, Magnetic penetration depth in $RbOs_2O_6$ studied by muon spin rotation, Phys. Rev. B **72**, 104504 (2005).

[55] R. Khasanov, P. W. Klamut, A. Shengelaya, Z. Bukowski, I. M. Savić, C. Baines, and H. Keller, Muon-spin rotation measurements of the penetration depth of the Mo_3Sb_7 superconductor, Phys. Rev. B **78**, 014502 (2008).

[56] N. Kurita, F. Ronning, C. F. Miclea, Y. Tokiwa, E. D. Bauer, A. Subedi, D. J. Singh, H. Sakai, J. D. Thompson, and R. Movshovich, Fully gapped superconductivity in Ni-pnictide superconductors $BaNi_2As_2$ and $SrNi_2P_2$, J. Phys.: Conf. Ser. **273**, 012097 (2011).

[57] X. C. Hong, Z. Zhang, S. Y. Zhou, J. Pan, Y. Xu, H. Wang, Q. Mao, M. Fang, J. K. Dong, and S. Y. Li, Multigap nodeless superconductivity in nickel chalcogenide $TlNi_2Se_2$, Phys. Rev. B **90**, 060504(R) (2014).

[58] F. Ronning, E. Bauer, T. Park, N. Kurita, T. Klimczuk, R. Movshovich, A. Sefat, D. Mandrus, and J. Thompson, Ni_2X_2 (X = pnictide, chalcogenide, or B) based superconductors, Physica C: Superconductivity **469**, 396 (2009).

[59] R. Khasanov, D. V. Evtushinsky, A. Amato, H.-H. Klauss, H. Luetkens, C. Niedermayer, B. Büchner, G. L. Sun, C. T. Lin, J. T. Park, D. S. Inosov, and V. Hinkov, Two-gap superconductivity in $Ba_{1-x}K_xFe_2As_2$: A complementary study of the magnetic penetration depth by muon-spin rotation and angle-resolved photoemission, Phys. Rev. Lett. **102**, 187005 (2009).

[60] R. Khasanov, M. Bendele, A. Amato, K. Conder, H. Keller, H.-H. Klauss, H. Luetkens, and E. Pomjakushina, Evolution of two-gap behavior of the superconductor $FeSe_{1-x}$, Phys. Rev. Lett. **104**, 087004 (2010).

[61] P. J. F. Cavalcanti, T. T. Saraiva, J. A. Aguiar, A. Vagov, M. D. Croitoru, and A. A. Shanenko, Multiband superconductors with degenerate excitation gaps, J. Phys.: Condens. Matter **32**, 455702 (2020).

[62] R. Gupta, C. Löhnert, C. Wang, D. Johrendt, H. Luetkens, S. Malick, T. Shiroka, Z. Hossain, and R. Khasanov, Isotropic *s*-wave superconductivity in the noncentrosymmetric charge density wave superconductor $SrPt_2As_2$, Phys. Rev. B **102**, 144515 (2020).

[63] A. Fente, E. Herrera, I. Guillamón, H. Suderow, S. Mañas-Valero, M. Galbiati, E. Coronado, and V. G. Kogan, Field dependence of the vortex core size probed by scanning tunneling microscopy, Phys. Rev. B **94**, 014517 (2016).

[64] A. Fente, W. R. Meier, T. Kong, V. G. Kogan, S. L. Bud'ko, P. C. Canfield, I. Guillamón, and H. Suderow, Influence of multiband sign-changing superconductivity on vortex cores and vortex pinning in stoichiometric high-T_c $CaKFe_4As_4$, Phys. Rev. B **97**, 134501 (2018).

[65] B.-H. Lei, Y. Guo, Y. Xie, P. Dai, M. Yi, and D. J. Singh, Complex structure due to As bonding and interplay with electronic structure in superconducting $BaNi_2As_2$, Phys. Rev. B **105**, 144505 (2022).